

# MedNeXt-v2: Scaling 3D ConvNeXts for Large-Scale Supervised Representation Learning in Medical Image Segmentation

Saikat Roy<sup>\*,1,2</sup>, Yannick Kirchhoff<sup>\*,1,2,3</sup>, Constantin Ulrich<sup>1,4,5</sup>, Maximillian Rokuss<sup>1,2</sup>,  
Tassilo Wald<sup>1,2,6</sup>, Fabian Isensee<sup>1,6</sup>, Klaus Maier-Hein<sup>1,2,7</sup>

<sup>1</sup>German Cancer Research Center (DKFZ) Heidelberg, Division of Medical Image Computing, Germany

<sup>2</sup>Faculty of Mathematics and Computer Science, Heidelberg University, Germany

<sup>3</sup>HIDSS4Health - Helmholtz Information and Data Science School for Health, Karlsruhe/Heidelberg, Germany

<sup>4</sup>Medical Faculty Heidelberg, Heidelberg University, Germany

<sup>5</sup>National Center for Tumor Diseases (NCT), Heidelberg, Germany

<sup>6</sup>Helmholtz Imaging, German Cancer Research Center, Germany

<sup>7</sup>Pattern Analysis and Learning Group, Department of Radiation Oncology, Heidelberg University Hospital, Germany

saikat.roy@dkfz-heidelberg.de; yannick.kirchhoff@dkfz-heidelberg.de

## Abstract

*Large-scale supervised pretraining is rapidly reshaping 3D medical image segmentation. However, existing efforts focus primarily on increasing dataset size and overlook the question of whether the backbone network is an effective representation learner at scale. In this work, we address this gap by revisiting ConvNeXt-based architectures for volumetric segmentation and introducing MedNeXt-v2, a compound-scaled 3D ConvNeXt that leverages improved micro-architecture and data scaling to deliver state-of-the-art performance. First, we show that routinely used backbones in large-scale pretraining pipelines are often suboptimal. Subsequently, we use comprehensive backbone benchmarking prior to scaling and demonstrate that stronger from scratch performance reliably predicts stronger downstream performance after pretraining. Guided by these findings, we incorporate a 3D Global Response Normalization module and use depth, width, and context scaling to improve our architecture for effective representation learning. We pretrain MedNeXt-v2 on 18k CT volumes and demonstrate state-of-the-art performance when fine-tuning across six challenging CT and MR benchmarks (144 structures), showing consistent gains over seven publicly released pre-trained models. Beyond improvements, our benchmarking of these models also reveals that stronger backbones yield better results on similar data, representation scaling dispro-*

*portionately benefits pathological segmentation, and that modality-specific pretraining offers negligible benefit once full finetuning is applied. In conclusion, our results establish MedNeXt-v2 as a strong backbone for large-scale supervised representation learning in 3D Medical Image Segmentation. Our code and pretrained models are made available with the official nnUNet repository at: <https://www.github.com/MIC-DKFZ/nnUNet>.*

## 1. Introduction

Automated segmentation of medical images is one of the most common tasks in biomedical image analysis [12, 28, 49, 52]. Despite rapid development in deep learning based approaches over the last decade [1, 42, 50], UNet-based [59] deep convolutional networks (ConvNets) have remained central to high-performing methodologies for 3D medical image segmentation [31, 32]. Although alternative approaches such as Transformers have been popular in recent years [36], their limited inductive bias has proved a hindrance for training from scratch on the currently available medical segmentation datasets, typically containing sparse annotations [42]. This has led to ConvNeXt-based [46] approaches leveraging the scalability of the Transformer

\*Contributed equally. Each author may denote themselves as positional first author in their CVs.

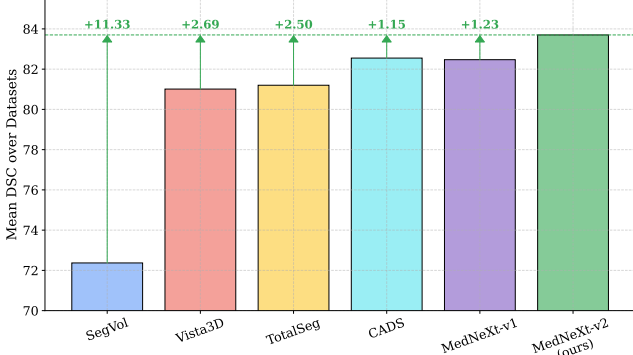


Figure 1. **MedNeXt-v2 sets a new state-of-the-art in 3D medical image segmentation.** By leveraging micro-architectural improvements and large-scale pretraining, it outperforms powerful existing networks across multiple 3D medical segmentation tasks.

while retaining the strong inductive bias of ConvNets to offer effective solutions for 3D medical image segmentation [10, 38, 43, 56, 61].

However, following significant advances in computer vision [13, 55, 66] over the last decade, the field of medical image segmentation has also been gradually moving towards incorporating large-scale supervised pretraining of deep networks [9, 26, 68, 72]. In recent years, the availability of large monolithic datasets [19, 73] or aggregated collections of previously available small-scale datasets [3, 39, 76] has led to initial attempts at pretraining large-scale deep learning models for the segmentation of 3D medical images. Notably, while approaches in 2D computer vision have moved towards self-supervised learning (SSL) owing to the abundance of unlabeled data [23, 34], the domain of 3D medical image segmentation continues to leverage supervised pretraining. Despite some initial SSL studies [70, 71] with 3D medical image pretraining, the efficiency in learning representations in supervised pre-training continues to be of interest. For example, in [40], it was demonstrated that supervised representation learning is 99.6% more data efficient than an SSL approach. However, annotated sample sizes remain limited compared to those of natural image datasets ( $O(10^4)$  vs  $O(10^7)$ ) [62], as the annotation of 3D medical images requires experienced radiologists and substantial costs arising from the substantial manual effort. Therefore, we consider *only supervised pre-training* in the course of this work. While initial attempts have proven effective [39, 40, 58, 68] for learning generalized representations, our work leads us to systemic issues with supervised pretraining in 3D medical image segmentation.

**Challenges in supervised pretraining:** Initial efforts towards the supervised pretraining of deep networks for medical image analysis have a number of recurring issues as shown in Tab. 1 – **P1) Legacy Backbones:** While large-

scale datasets in natural image analysis are more established, such as ImageNet, MS-COCO, ADE20k [14, 41, 77], the construction of large medical image datasets is a vigorously active area of research [8, 19, 21, 54, 76]. Therefore, owing to dataset creation itself being an active line of research, many recent efforts share a limitation in solely emphasizing on dataset scale, often aiming to demonstrate the efficacy of their large pretraining corpora on *any* deep architecture in general, but not necessarily combining it with a state-of-the-art network for 3D medical image segmentation (4 out of 11 cases). **P2) Scaling data after backbone validation:** The preceding problem could, in theory, be eliminated by benchmarking the backbone architecture prior to pretraining. However, as seen in Tab. 1, this is not usually performed (2 out of 11 cases) – but as shown later in Tab. 4, stronger backbones lead to stronger pretrained networks. **P3) Comparisons against only from-scratch baselines:** Finally, we observe that large-scale pretrained models are usually evaluated solely against models trained from scratch. While this does indeed highlight the benefits of pretraining in general, it does little to highlight the effectiveness of a *specific* pretraining strategy. We observe that 4 out of 11 surveyed methods evaluate against other pretrained methods, leading to questions of effectiveness of such methods as pretrained backbones.

In this work, we attempt to bridge this gap by shifting the focus from dataset size alone to representation quality by asking: *“Is our large-scale representation learner suitable for learning effective representation from dataset scaling?”*. In doing so, we offer a ConvNeXt-based architecture for state-of-the-art 3D medical image segmentation. Our contributions can be expressed as combination of validating our network for effective small-scale segmentation performance *prior to* pairing it with effective large-scale pretraining and downstream evaluation, as follows:

1. **Backbone Validation:** The standard approach of selecting networks for effective large-scale representation learning for medical images is seemingly selecting the best off-the-shelf network available based on external baselines [19, 21, 73, 76] or using their own proposed network with limited small-scale evaluations [30]. A lack of focus in this direction [8] can also lead to the selection of methods for large-scale training, which have notably worse performance against state-of-the-art methods in multiple benchmarks [4, 32]. To address this, we propose to actively benchmark our network on effective segmentation performance for multiple pathological and anatomical structures on *multiple* small-scale 3D datasets. Subsequently, we demonstrate that benchmarking performance correlates strongly to downstream performance following pretraining. (Sec. 2.1)
2. **Leveraging large-scale pretraining of ConvNeXts:** We introduce MedNeXt-v2, which is a ConvNeXt-based

[74] architecture, for state-of-the-art 3D medical image segmentation. However, we do not claim complicated architectural innovations. Instead, we leverage sensible micro-architectural improvements via a 3D Global Response Normalization (GRN) module and combine it with large-scale pretraining on 18k 3D CT volumes on 40 structures. To increase the efficacy of fine-tuning, we demonstrate that a simple increase in input context during a short fine-tuning phase is able to outperform 7 equivalently trained large-scale competitive baselines (some trained on more data, or larger size) on 6 challenging CT and MR downstream segmentation tasks on 144 structures as summarized in Fig. 1. (Sec. 4.1)

3. **Benchmarking of large-scale supervised pretraining in medical image segmentation:** Finally, large-scale pretraining of 3D medical image segmentation networks is an relatively newer and active area of research. Accordingly, there is limited availability of benchmarks specifically for downstream fine-tuning to draw generalized conclusions for 3D supervised pretraining. In this work, we are the first to benchmark seven publicly available large-scale pretrained networks for 3D medical image segmentation and compare it against 3 networks proposed by us. We derive insights about the influence of pretraining backbones on downstream finetuning performance, the effectiveness of modality-specific pretraining and anatomy-specific performance gains. (Sec. 4.2)

## 2. Method

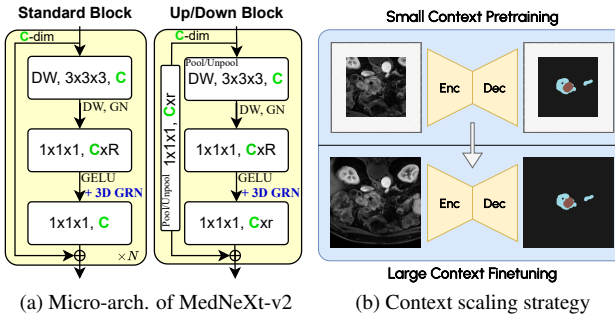


Figure 2. **Network Improvements.** Our network scaling targets the base number of channels (C) while **3D GRN** improves the micro architecture by limiting activation saturation or collapse during training. Also shown is our context scaling strategy.

### 2.1. Scaling data only after validating backbones

One of our interesting findings is that 9 out 11 large-scale methods that we have explored in Tab. 1 do not perform any validation of the backbone before introducing data scaling. This introduces performance-based challenges during downstream fine-tuning of a backbone, especially when

Methods	Backbones	Venues	P1	P2	P3
<b>M01</b> [72]	ViT	ECCV'23	✗	✗	✗
<b>M02</b> [26]	SegResNet	CVPR'25	✗	✗	✗
<b>M03</b> [73]	nnUNet	Rad:AI'23	✗	✗	✗
<b>M04</b> [19]	nnUNet	Rad'25	✗	✗	✗
<b>M05</b> [21]	ResEncL	EuroRad'25	✗	✗	✗
<b>M06</b> [76]	ResEncL	arXiv'25	✗	✗	✗
<b>M07</b> [8]	SwinUNETR	ICCV'25	✗	✗	✗
<b>M08</b> [40]	SwinUNETR	ICLR'24	✗	✗	✗
<b>M09</b> [64]	SwinUNETR	MICCAI'23	✗	✗	✗
<b>M10</b> [44]	SwinUNETR	MedIA'24	✗	✗	✗
<b>M11</b> [20]	(Res) UNet	ICCV'24	✗	✗	✗

Table 1. **Systemic gaps in large-scale 3D medical image segmentation.** **P1: Legacy architectures.** Many large-scale studies default to popular baselines (e.g., nnU-Net), treating architecture as fixed and focusing the problem to “more data,” while underusing stronger representation learners. **P2: Scaling data after Backbone validation.** Almost *universally*, architectures are ported *directly* to large-scale training with *limited or no* small-scale benchmarking – implicitly assuming that more data will yield strong performance. This assumption has no guarantees and excludes architecture that could have benefited more from pretraining. **P3: Only non-pretrained baselines.** Finally, large-scale pretrained models are sometimes evaluated only against baselines trained from scratch, thereby undercutting comparisons to *true* state-of-the-art. Here, ✗ represents the presence of a problem.

fine-tuning for clinical purposes leveraging automated segmentation such as radiotherapy planning [53] or target localization in biopsies [65] – namely, a weak backbone will be restricted to weaker pretrained representations. In this work, we propose validating our backbone against existing state of the art architectures on 4 public validation datasets – BTCV [37], AMOS22 [33], KITS21 [27] and ACDC [5] (more in Sec. D.1). We choose the 5 architectures used in backbones in Tab. 1 and 3 state-of-the-art architectures from recent medical image segmentation benchmarks [4, 32].

As demonstrated in Tab. 2 based on Dice Similarity Coefficient (DSC) that MedNeXt [61] is the best performing network *from literature*, with ResEncL [32] being a close second. In fact, ResEncL is considered to be a state-of-the-art architecture in literature based on its performance [4], but is only used by 2 out 11 large-scale pretrained nets in Tab. 1. This highlights that **a)** Regular benchmarking (or consulting *latest* benchmarking initiatives) for backbones prior to data scaling should be encouraged for better large-scale pretraining, **b)** MedNeXt is an effective architecture for further development, as shown by the best performance of our newly introduced MedNeXt-v2 in the same benchmark in Tab. 2.

Backbones	BTCV	AMOS	KITS	ACDC	AVG
<b>Existing backbones as in Tab. 1</b>					
<b>UNETR (ViT)</b>	73.11	79.71	80.81	91.38	81.25
<b>SegResNet</b>	80.22	86.83	83.34	92.38	85.69
<b>nnUNet</b>	79.84	87.95	87.67	93.34	87.20
<b>SwinUNETR</b>	77.20	85.39	85.09	92.59	85.07
<b>ResEnc-L</b>	80.66	<b>88.12</b>	88.25	<u>93.44</u>	87.62
<b>State of the Art backbones as in [4, 32]</b>					
<b>CoTr</b>	78.17	87.05	85.39	<b>93.47</b>	86.02
<b>STU-Net</b>	80.24	87.67	87.02	93.15	87.02
<b>MedNeXt-v1</b>	<b>81.02</b>	88.02	<u>88.84</u>	93.08	<u>87.74</u>
<b>MedNeXt-v2</b>	80.99	88.05	<b>89.09</b>	93.39	<b>88.03</b>

Table 2. **Benchmarking before Data Scaling.** While there is a limited history of benchmarking backbones [8, 20] before dataset scaling, this step is usually ignored and as demonstrated, to potentially negative consequences. In fact, we demonstrate that 4 out of 5 architectures used in Tab. 1, are outperformed by easy to train but better representation learners such as ResEncL or MedNeXt-v1 on 4 public datasets, with SOTA architectures derived from recent large-scale benchmarking studies for 3D medical image segmentation [4, 32]. This ineffectiveness of using sub-par backbones for learning generalized representations, therefore, weakens the models paired with such large-scale 3D medical image datasets. **Bold:** Best results, Underline: Second-best results.

## 2.2. MedNeXt-v2: Compound scaling ConvNeXts

MedNeXt (henceforth referred to as MedNeXt-v1) is a popular ConvNeXt-based architecture for 3D medical image segmentation effective in representation learning on small-scale as well as large scale training. In essence, it is designed as a 5-layer UNet [59] with ConvNeXt blocks at every layer of the network (further in Sec. B). Our goal is to sensibly scale the architecture and training data to obtain a MedNeXt-v2 variant capable of learning stronger representations in 3D medical image datasets. We also aim to enable finetuning of this model at a fractional of the training compute, thereby allowing rapid adoption in downstream segmentation tasks. MedNeXt-v1 leveraged the idea of compound scaling from EfficientNet [67] to simultaneously scaling multiple components of the network. We further modify the network micro-architecture and scale along these lines, as described in the following sections.

### 2.2.1. 3D Global Response Normalization (GRN)

2D GRN was a micro-architectural component introduced in the ConvNeXt-V2 [74] in the natural image domain to prevent feature collapse in training ConvNeXt networks. The position of these blocks post the expansion layer encourages the learning of diverse representations by preventing overly dominant feature maps, as the expansion ratio is increased. We adopt it as a 3D GRN block with  $l2$  normalization for a volumetric feature map  $X_i = \gamma * X_i * \mathcal{N}(X_i)$

$\beta + X_i \in \mathcal{R}^{H \times W \times D}$  where  $\mathcal{N}(X_i) = \frac{\|X_i\|}{\sum_{j=1}^C \|X_j\|} \in \mathcal{R}$  for  $C$ -channels and  $\beta, \gamma$  are learnable parameters. We incorporate GRN in all 3D MedNeXt blocks across our architecture for effective pretraining and fine-tuning performance. Additionally, we ablate our choice of 3D GRN on the same settings as our backbone validation in Tab. 3, as well as the effect on activations following fine-tuning in Tab. 3, further demonstrating the effectiveness of the module.

Table 3. **3D GRN improves segmentation performance in MedNeXt-v2.** 3D GRN in our MedNeXt-v2 stabilizes performance on average (*always* best or second-best) and gives an edge over both MedNeXt-v1 and SOTA baselines when training from-scratch, leading to higher gains following large-scale pretraining (Fig. 4). **Bold:** Best results, Underline: Second-best results.

Model	BTCV	AMOS	KiTS	ACDC	Mean
nnUNet	79.84	87.95	87.67	93.34	87.20
ResEncL	80.66	<b>88.12</b>	88.25	<b>93.44</b>	87.62
MedNeXt-v1	<b>81.02</b>	88.02	<u>88.84</u>	93.08	87.74
MedNeXt-v2	80.99	88.05	<b>89.09</b>	<u>93.39</u>	<b>88.03</b>

### 2.2.2. Scaling of ConvNeXt Nets

We work to establish the idea of scaled networks paired with large-pretraining data. We investigate varying degrees of scaling enabled by the MedNeXt-v2 micro architecture. They are as follows:

- **Depth Scaling:** We adopt the 52 layer depth of the original large (L) variant of MedNeXt-v1 for the default depth level of our v2 architecture. We maintain this scaling *throughout all our experiments*.
- **Width Scaling:** Standard ResNet-like blocks allow for increases in channel size. We perform width scaling via increasing the base channel size to  $2C$ , thereby doubling capacity, while maintaining the  $R$  to values as in MedNeXt-v1 [61].
- **Context Scaling:** 3D deep segmentation networks typically leverage patch-based training for limiting VRAM consumption (similar to other tasks in medical image analysis [11, 29, 60, 63]), where patch size limits the degree of available context for the deep network. While smaller patch sizes of  $96 \times 96 \times 96$  or  $128 \times 128 \times 128$  [24, 38, 61] have become commonplace, this limits performance on certain tasks. We scale the patch size to  $192 \times 192 \times 192$  as one of our scaling investigations to increase available context to our network during finetuning.

**Limiting Input Context during pretraining.** There is a dichotomy in scaling of input context by increasing patch size in 3D medical images. On the one hand, it is fundamentally beneficial to leverage larger input context for better performance. However, using large patch sizes in

large-scale 3D architectures is memory-intensive and requires significant compute. However, we find it effective to use the standard input patch size of  $128 \times 128 \times 128$  in pretraining, and scale it up to  $192 \times 192 \times 192$  during fine-tuning. This is effective as our pipeline favors rapid fine-tuning (300 epochs) which is 20% of the pretraining schedule.

### 2.3. Data-Scaling via Large Scale Pretraining

As mentioned in Sec. 2.3, large-scale pretraining has been one of the drivers of computer vision research over the last decade [57, 66]. Accordingly, to enable generalization across diverse imaging domains with varying texture, contrast and noise characteristics, we pretrain our model on 18k images of the publicly available subset of the CADS data collection [76]. We select a subset of 44 target structures from the available labels thereby simplifying the granularity of the original dataset while ensuring wide anatomical coverage to learn effective generalized representations without optimizing for fine-grained details. This is suitable given our intention to fine-tune our network on downstream tasks.

**Pretraining strategy** For pretraining, we use the nnUNet framework [31] to optimize our model across 4 A100 GPUs with distributed data parallel training. The models are trained for 1500 epochs with 250 batches per epoch, a batch size of 8 (2 per GPU) and a patch size of  $128 \times 128 \times 128$ . We use the AdamW optimizer [47] used in the original MedNeXt [61] with linear weight decay and an initial learning rate of 1e-3. We use the default nnUNet preprocessing, data augmentations, loss etc in the course of the pretraining.

**Fine-tuning strategy** The relatively recent introduction of large-scale architectures in 3D medical image segmentation often sees them used in conjunction with optimizers which do not specifically account for convergence stability early in training – for example, SGD in [30, 32] with networks as large as 1.4B Parameters and 12.6 TFLOPS. To stabilize our fine-tuning, we add Linear Warmup [45] of 50 epochs to the AdamW optimizer with a maximum learning rate of 1e-3 and fine-tune for a total of 300 epochs with 250 random batches of size 2 per epoch. We use a patch size of  $128 \times 128 \times 128$  unless otherwise stated.

## 3. Experimental Setup

### 3.1. Datasets

**Initial Benchmarking Datasets** We use 4 datasets as explored in [32] for our backbone benchmarking and GRN validations prior to data scaling. Our datasets consist of diverse target structures, imaging modalities and training set sizes - 1) Beyond-The-Cranial-Vault (BTCV) organ segmentation CT dataset [37], 2) AMOS Organ Segmentation

(AMOS22) CT Dataset [33], 3) MICCAI Kidney Tumor Segmentation Challenge 2023 (KiTS23) [27] CT dataset and 4) Automatic Cardiac Diagnostic Challenge (ACDC) [5] CINE MR dataset to develop our methods, with 30, 200, 489 and 200 samples respectively. We use z-score normalization on all datasets and resample them to isotropic spacing. Results on these datasets are expressed as Dice Similarity Coefficient (DSC) as in Tabs. 2 and 3 on a 80-20 data split strategy for training and validation sets.

**Final Evaluation Datasets** We use 5-fold cross validation for our final evaluation providing Dice Similarity Coefficient (DSC) and Normalized Surface Distance (NSD) at 1mm tolerance on a diverse and challenging set of six public datasets across CT and MR modalities to perform our evaluation. Similar to our initial backbone benchmarking, we use z-score normalization on all datasets and resample them to isotropic spacing. They are described as follows:

1. *Pediatric CT-Seg* [35] (D1): Pediatric CT exams with expert organ contours from multiple institutions and scanners.
2. *Stanford Knee MR* [16] (D2): Manual segmentations of six knee tissues: patellar and femoral cartilage, lateral/medial tibial cartilage, and lateral/medial meniscus.
3. *Toothfairy* [7, 48] (D3): CBCT volumes with 77-class dental segmentations, including teeth, canals, jaws, and implants.
4. *Stanford Brain Mets* [22] (D4): brain MRI studies with radiologist-annotated brain metastases segmentations across multiple sequences.
5. *PANTHER Pancreatic Tumor* [6] (D5): T1-weighted contrast-enhanced pancreatic MRIs with pancreas and tumor annotations.
6. *CTSpine1k* [15] (D6): Large-scale spine CT dataset expert-labeled vertebrae. We exclude all samples from the popular Liver Tumor Segmentation [2] task from this dataset to prevent overlaps with pretraining cohorts of AbdomenAtlas1.0 in Tab. 4.

### 3.2. Large-scale Pretrained Baselines

We use seven publicly available pretrained methods for both benchmarking their performance against each other and as a baseline against our pretrained MedNeXt-v2 architectures. We use TotalSegmentator (TotalSeg) [73], MRSegmentator (MRSeg.) [19], CADS [76], the segmentation backbone of Vista3D [26], the pretrained ViT backbone of SegVol [18] incorporated in an UNETR decoder [25], STU-Net [30] and the original MedNeXt-v1 [61]. Only the last 2 among these 7, namely STU-Net and MedNeXt-v1, were not introduced accompanied by a large-scale pretraining dataset and were pretrained on the AbdomenAtlas1.0 dataset [54] as part of the Touchstone large-scale medical image segmentation benchmark [4]. The remaining 5 were trained on the

same datasets they accompanied when they were proposed. We use the fine-tuning strategy as described in Sec. 2.3 for all methods for fair comparison against MedNeXt-v2 with a patch size of  $128^3$  similar to our base MedNeXt-v2. However, we maintain the nnUNet-proposed large patch size of CADS on each dataset for fairer comparison as its ResEncL backbone depends on increased patch size for performance.

### 3.3. Scaled MedNeXt-v2 variants

We experiment with three variants of our MedNeXt-v2 representing different forms of scaling which are as follows:

1. **Base Network:** This is the base variant of our proposed MedNeXt-v2 architecture which follows the large (L) configuration of the MedNeXt-v1 with an added GRN module for improved representation learning.
2. **Patch  $\times 1.5$ :** The base network performs pretraining and fine-tuning with a patch size of  $128 \times 128 \times 128$ . In this variant of the network, we scale the patch side length by 1.5 times to  $192 \times 192 \times 192$  for the fine-tuning schedule.
3. **Width  $\times 2.0$ :** In this variant, the number of channels of the base network is increased by a factor of two at each stage of the network. This effectively doubles network capacity of the wide configuration compared to the base network.

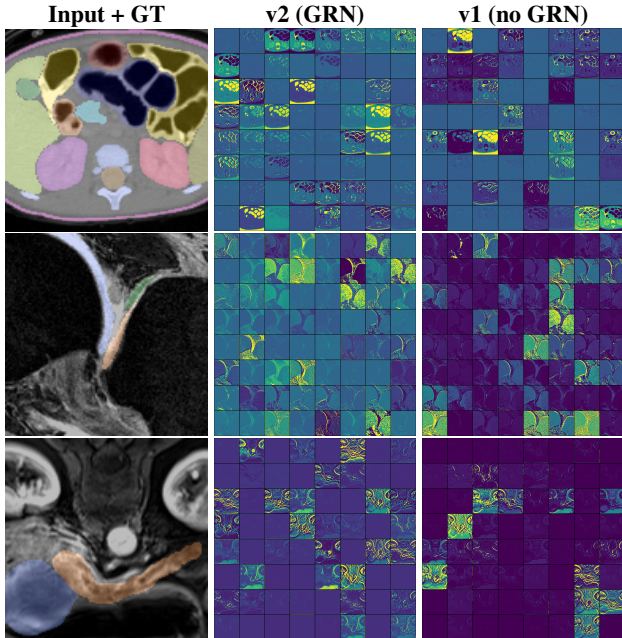


**Figure 3. Channel activation visualization demonstrates that 3D GRN reduces redundant activations.** Akin to ConvNeXt-v2 [74], our visualization of 64 activations in layer 1 of MedNeXt-v2 (with GRN) and MedNeXt-v1 (without GRN) on Pediatric-CT (D1), Stanford Knee (D2) and Pancreatic Tumor (D5) from Tab. 4 demonstrates that 3D GRN prevents dead or saturated activations in 3D medical image segmentation tasks, preventing feature collapse and aiding representation learning.

## 4. Results and Discussion

### 4.1. MedNeXt-v2 is state-of-the-art for 3D medical image segmentation

MedNeXt-v2 leverages micro-architectural improvements and data scaling to demonstrate state-of-the-art performance for 3D medical image segmentation. We discuss the nuances of our performance against MedNeXt-v1 as well as seven other large-scale pretrained baselines. We also discuss the merits of using higher network capacity and larger input context during finetuning in the following sections.

**Improvement over MedNeXt-v1.** As illustrated in Fig. 4, the integration of a GRN module delivers consistent improvements over MedNeXt-v1, with and without pretraining. This is owing to a similar phenomenon as in ConvNeXt-v2 of preventing feature collapse represented by dead or saturated neuron which we visualize in Fig. 3. Across 144 structures on 6 challenging public datasets spanning CT and MR modalities, MedNeXt-v2 demonstrates state-of-the-art performance. On challenging datasets for Pediatric CT Segmentation (D1) and pancreatic tumor segmentation (D5), it achieves gains of up to **+1.0 DSC** despite saturated accuracy ceilings, affirming MedNeXt-v2 as an architecture for effective representation learning in 3D medical image segmentation.

**SOTA among pretrained baselines** All MedNeXt-v2 variants are seen to outperform *all seven large-scale pretrained baselines* in Tab. 4. This includes average gains of **+2.69 DSC**, **+2.97 NSD** and **+1.15 DSC**, **+1.46 NSD** respectively over powerful pretrained networks like Vista3D and CADS, as illustrated in Fig. 6, demonstrating MedNeXt-v2 as a state-of-the-art large-scale pretrained backbone. In particular, our outperforming of CADS on similar pretraining data demonstrates the benefits of the ConvNeXt architecture as a superior backbone for leveraging large annotated pretraining datasets (see also Sec. 4.2) for downstream segmentation tasks across CT as well as MR modalities.

**Scaling context during finetuning** Our increase in side length of the input patch to  $192^3$  increases the spatial context available to MedNeXt-v2 by  $3.375\times$ . This results in a successful scaling strategy and performance is seen to improve in numerous datasets leveraging this spatial context. In particular, we offer an illustration in Fig. 5 on Toothfairy dataset (D3) where this extra context is seen to help with the segmentation of a structure (*tooth*) by possibly leveraging the spatial position of the nearby anatomy (*jaw*). Quantitatively, we see large improvements on D3 of **+1.43 DSC** and **+3.57** on D1 (Pediatric CT-Seg) against other pretrained methods. While our large input patch variant MedNeXt-v2

Table 4. **MedNeXt-v2 demonstrates state-of-the-art performance across 144 structures against existing pretrained baselines.** We validate our methods on 6 diverse datasets (3 CT and 3 MR) across 144 anatomical and pathological structures. We demonstrate state-of-the-art segmentation performance based on both DSC and NSD against 7 large-scale pretrained networks. We are also the first to systematically benchmark large-scale pretrained networks at scale and offer significant insights for such models (Sec. 4.2). **Bold:** Best results, **Underline**: Second-best results.

Pretrained Models	Pretraining Datasets	Dice Similarity Coefficient (DSC)						D6	Mean
		D1	D2	D3	D4	D5			
<b>Training from Scratch</b>									
<b>nnUNet</b> [31]	-	79.81/74.93	87.28/87.37	85.63/88.89	65.37/77.23	68.70/45.31	96.63/97.22	80.57/78.49	
<b>ResEncL</b> [32]	-	82.62/78.39	87.03/87.06	88.55/91.47	65.67/77.81	69.11/46.05	96.89/97.57	81.65/79.72	
<b>MedNeXt-v1</b> [61]	-	84.28/80.22	87.26/87.47	89.38/92.29	64.87/77.73	69.37/46.49	<u>97.12</u> /97.74	82.05/80.32	
<b>MedNeXt-v2</b>	-	<u>84.84</u> /80.74	87.16/87.33	89.49/92.40	64.89/77.04	70.41/46.81	97.06/97.70	82.31/80.34	
<b>Pretrained Baselines (using Publicly Available Weights)</b>									
<b>TotalSeg.</b> [73]	TotalSeg-CT	77.60/72.19	87.19/87.17	86.74/90.18	67.85/80.21	71.74/46.83	96.11/96.60	81.20/78.86	
<b>MRSeg.</b> [19]	TotalSeg-MR	78.41/73.19	87.29/87.32	87.54/90.98	67.02/79.17	71.62/46.50	96.21/96.72	81.35/78.98	
<b>CADS</b> [76]	CADS-Organ	81.74/77.27	87.08/87.16	<u>90.34</u> /93.37	68.07/79.69	71.32/47.04	96.75/97.36	82.55/80.31	
<b>Vista3D</b> [26]	Vista	78.78/73.70	87.18/87.13	87.75/91.30	65.85/77.89	70.03/45.83	96.44/96.95	81.01/78.80	
<b>SegVol</b> [18]	SegVol	73.95/65.98	85.63/84.37	74.19/78.15	51.10/62.08	60.24/34.71	89.10/88.56	72.37/68.97	
<b>STUNet-L</b> [30]	Abd.Atlas1.0	80.70/76.18	87.12/87.18	88.61/91.82	66.15/77.69	<u>71.99</u> /47.53	96.40/96.94	81.83/79.56	
<b>MedNeXt-v1</b> [4]	Abd.Atlas1.0	82.02/77.81	<u>87.33</u> /87.55	89.09/92.03	68.52/80.21	71.01/47.88	96.81/97.39	82.47/80.52	
<b>MedNeXt-v2 (Our Pretrained Weights)</b>									
<b>Base Network</b>	CADS-sub	83.15/79.12	87.28/87.45	89.29/92.43	<b>69.04/81.23</b>	71.93/48.49	97.03/97.62	<u>82.95</u> /81.06	
<b>Patch <math>\times</math> 1.5</b>	CADS-sub	<b>85.59/81.72</b>	87.15/87.26	<b>91.77/94.59</b>	68.12/80.26	<b>72.38/48.93</b>	<b>97.20/97.87</b>	<b>83.70/81.77</b>	
<b>Width <math>\times</math> 2.0</b>	CADS-sub	83.62/79.81	<b>87.35/87.57</b>	89.44/92.44	67.03/79.42	71.94/48.12	97.04/97.68	82.74/80.84	

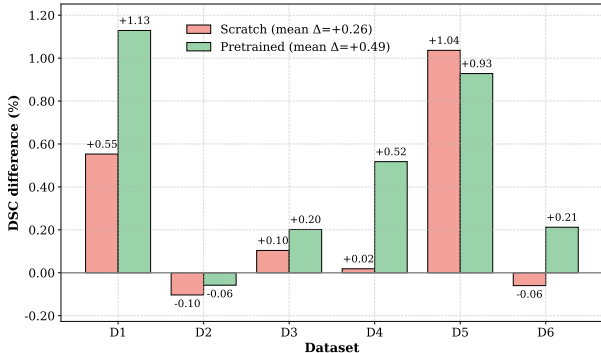


Figure 4. **MedNeXt-v2 outperforms MedNeXt-v1 from scratch and during finetuning.** The addition of the GRN stabilizes the performance of the v2 architecture and improves performances compared to MedNeXt-v1 as seen in Tab. 4. We see improvements  $>1.0$  Dice points on tasks as diverse as the segmentation of Pediatric Organs in CTs (**D1**) and Pancreatic Tumor in MR (**D5**). We only observe limited gains on the highly saturated knee segmentation task **D2** for all methods.

performs the best in our benchmark, we do not attribute any unfair advantage to our network. CADS, for example, leverages a large input patch size as well but does not show performance as strong as MedNeXt-v2. The combination of a strong backbone and larger input patches benefits MedNeXt-v2 in achieving strong downstream performance.

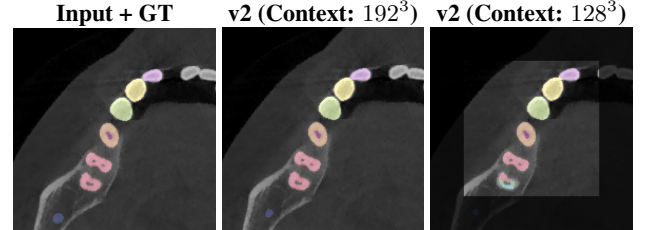


Figure 5. **Increased context during fine-tuning improves performance.** Increasing the available spatial context to 3.375 times with  $192^3$  patches is a cheap and effective strategy to leverage our pretrained MedNeXt-v2 while limiting pretraining costs. Importantly, we see an example from Toothfairy (D3) where added spatial context of the jaw enables better segmentation of the teeth near the image boundary, which a MedNeXt-v2 fine-tuned on  $128^3$  patches is unable to segment accurately.

**Scaling Capacity** We obtain mixed results with scaling capacity (Width  $\times 2.0$ ) during pretraining and fine-tuning. Doubling the base channel capacity of the 52-layer base network increases parameters from 62M to 247M and its usage during pretraining massively scales required compute. However, while we see superior performance on average to all seven existing pretrained baselines during finetuning on both DSC and NSD, it does not exceed the performance of the smaller MedNeXt-v2 base network or the MedNeXt-v2 with larger input patch scaling. Coupled with the limited performance of 440M parameter STU-Net, this motivates

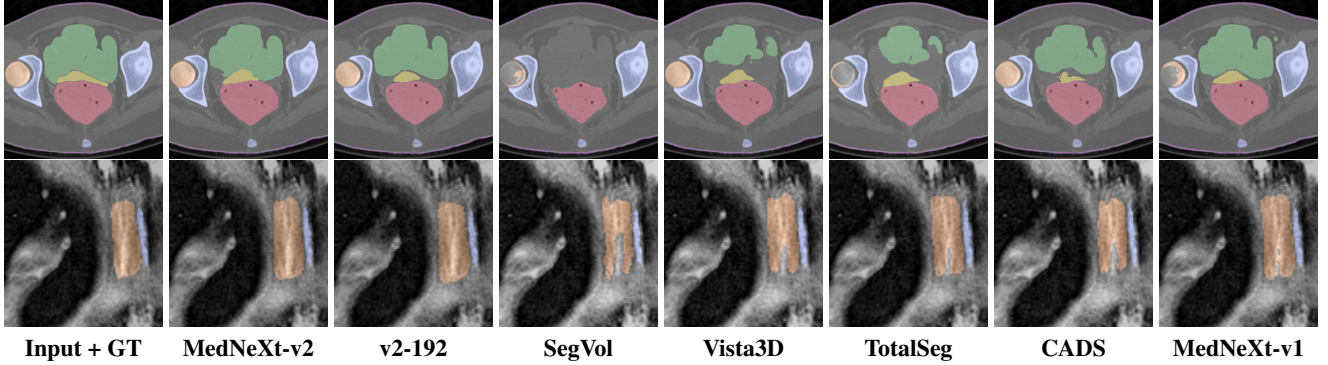


Figure 6. **Qualitative visualizations.** We visualize 1 CT (D1: Pediatric CT-Seg) and 1 MR (D2: Stanford Knee MR) dataset to demonstrate the effectiveness of MedNeXt-v2 and MedNeXt-v2 with large  $192^3$  context against other pretrained baselines including MedNeXt-v1.

us to reflect on naively scaling network capacity in the face of existing pretraining dataset sizes in Sec. E.

## 4.2. Benchmarking Analysis

Our benchmarking of existing large-scale backbones for 3D medical image segmentation offers significant insights and constitutes one of the first systematic evaluations of fine-tuning these architectures.

**Better backbones lead to better pretraining** In our backbone validation in Tab. 2, we hypothesized that better performance from scratch would lead to improvements in pretraining (and consequently during finetuning). We demonstrate that this is indeed the case when comparing the performance of CADS (ResEncL) and MedNeXt-v2 in Tab. 4. Both are similarly pretrained, but the performance from-scratch is carried through with MedNeXt-v2 outperforming the CADS (ResEncL) model, by margins as large as **+1.0 DSC** on segmenting small ( $< 0.05\text{cm}^3$ ) metastatic lesions [69] in brain MRIs (D4). This is not restricted to a single modality as similar performance (**+1.4 DSC**) is also seen when segmenting organs in pediatric CTs (D1), with equivalent gains in NSD indicating accurate surface delineation. This highlights that the choice of backbone is key to taking advantage of large pretraining datasets for accurate downstream segmentation performance.

### General Pretraining vs Modality-Specific Pretraining

A key finding from our benchmark is the comparison between TotalSeg-CT and MR, which use CT and MR pre-training, respectively, while sharing a similar nnU-Net backbone. Pretraining yields substantial gains, exceeding **+2.0 DSC** on brain metastasis (D4) and pancreatic tumor segmentation (D5) compared to training from scratch. However, the two models remain nearly indistinguishable across CT and MR evaluation datasets in terms of DSC and NSD. This raises the question of the effectiveness of

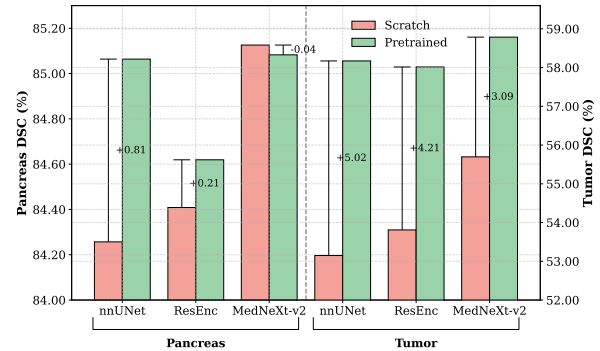


Figure 7. **Tumor classes benefit massively in pretraining.** Our analysis on Pancreatic Tumor Segmentation dataset (D4) in Tab. 4 demonstrate that across multiple networks, the benefit of pretraining in accurate tumor segmentation is significantly more than for the segmentation of the pancreas.

*isolated* modality-specific pretraining, suggesting that for structurally similar modalities (e.g., CT, MR, PET-CT), learned representations generalize well across modalities, thereby making the effect of modality-specific pretraining inseparable from standard pretraining.

**Tumors vs Healthy Structures** To better understand the role of pretraining in the segmentation of pathological versus non-pathological structures, we use pancreatic tumor segmentation (D5) as a representative case. We compare three pretrained models, namely TotalSegmentator-CT (nnU-Net), CADS (ResEncL), and MedNeXt-v2 (base) against their from-scratch counterparts, as shown in Fig. 7. In doing so, we observe two consistent trends:

- Across all backbones, pretraining yields substantial improvements on the *tumor class*, with MedNeXt-v2 achieving the highest absolute performance but the smaller nnU-Net backbone exhibiting the largest relative gain of approximately **+5.0 DSC**.

- For *organ segmentation*, results are more mixed with the larger networks showing moderate to no gains following pretraining. However, smaller backbones are again seen to benefit the most.

These findings suggest that *pathological segmentation tasks benefit disproportionately from large-scale pretraining*, and may in fact serve as more discriminative benchmarks for evaluating generalization than the segmentation of healthy anatomical structures.

## 5. Conclusion

Developing deep learning architectures that perform reliably across the wide variety of 3D medical image segmentation tasks [31] remains challenging. Although training from scratch has dominated the field over the past decade, methodological advances often focused on gains in small-scale data regimes. In this work, we embrace the shift toward large-scale supervised representation learning and introduce MedNeXt-v2, a pretrained ConvNeXt-based architecture that achieves state-of-the-art performance in 3D medical image segmentation. We validate our design against seven pretrained baselines and derive several key insights from what is, to our knowledge, one of the first systematic evaluations of publicly available pretrained methods with an emphasis on downstream finetuning. We hope that our findings, along with our open-source code and pretrained models, will foster further research in this direction.

## Acknowledgements

The present contribution is supported by the Helmholtz Association under the joint research school "HIDSS4Health – Helmholtz Information and Data Science School for Health". This work was partly funded by Helmholtz Imaging (HI), a platform of the Helmholtz Incubator on Information and Data Science.

The authors also gratefully acknowledge the computing time provided on the high-performance computer HoreKa by the National High-Performance Computing Center at KIT (NHR@KIT). This center is jointly supported by the Federal Ministry of Education and Research and the Ministry of Science, Research and the Arts of Baden-Württemberg, as part of the National High-Performance Computing (NHR) joint funding program (<https://www.nhr-verein.de/en/our-partners>). HoreKa is partly funded by the German Research Foundation (DFG). This work was supported by the Helmholtz Association's Initiative and Networking Fund on the HAICORE@FZJ partition.

Finally, we would like to wholeheartedly acknowledge the help of our colleagues at the German Cancer Research Center (DKFZ), namely, Balint Kovacs, Katharina Eckstein and Moritz Langenberg for their invaluable help towards the completion of this manuscript.

## References

- [1] Mohamed A Abdou. Literature review: Efficient deep neural networks techniques for medical image analysis. *Neural Computing and Applications*, 34(8):5791–5812, 2022. [1](#)
- [2] Michela Antonelli, Annika Reinke, Spyridon Bakas, Keyvan Farahani, Annette Kopp-Schneider, Bennett A Landman, Geert Litjens, Bjoern Menze, Olaf Ronneberger, Ronald M Summers, et al. The medical segmentation decathlon. *Nature communications*, 13(1):4128, 2022. [5](#)
- [3] Fan Bai, Yuxin Du, Tiejun Huang, Max Q. H. Meng, and Bo Zhao. M3d: Advancing 3d medical image analysis with multi-modal large language models, 2024. [2](#)
- [4] Pedro RAS Bassi, Wenzuan Li, Yucheng Tang, Fabian Isensee, Zifu Wang, Jieneng Chen, Yu-Cheng Chou, Yannick Kirchhoff, Maximilian R Rokuss, Ziyan Huang, et al. Touchstone benchmark: Are we on the right way for evaluating ai algorithms for medical segmentation? *Advances in Neural Information Processing Systems*, 37:15184–15201, 2024. [2](#), [3](#), [4](#), [5](#), [7](#), [14](#), [15](#)
- [5] Olivier Bernard, Alain Lalande, Clement Zotti, Frederick Cervenansky, Xin Yang, Pheng-Ann Heng, Irem Cetin, Karim Lekadir, Oscar Camara, Miguel Angel Gonzalez Ballester, et al. Deep learning techniques for automatic mri cardiac multi-structures segmentation and diagnosis: is the problem solved? *IEEE transactions on medical imaging*, 37(11):2514–2525, 2018. [3](#), [5](#)
- [6] Amparo Soeli Betancourt Tarifa, Faisal Mahmood, Uffe Bernchou, and Peter Jan Koopmans. Panther challenge: Public training dataset, 2025. [5](#)
- [7] Federico Bolelli, Luca Lumetti, Shankeeth Vinayahalingam, Mattia Di Bartolomeo, Arrigo Pellacani, Kevin Marchesini, Niels Van Nistelrooij, Pieter Van Lierop, Tong Xi, Yusheng Liu, et al. Segmenting the inferior alveolar canal in cbct volumes: the toothfairy challenge. *IEEE Transactions on Medical Imaging*, 2024. [5](#)
- [8] Emmanuelle Bourigault, Amir Jamaludin, and Abdullah Hamdi. Ukbob: One billion mri labeled masks for generalizable 3d medical image segmentation. *arXiv preprint arXiv:2504.06908*, 2025. [2](#), [3](#), [4](#)
- [9] Victor Ion Butoi, Jose Javier Gonzalez Ortiz, Tianyu Ma, Mert R Sabuncu, John Guttag, and Adrian V Dalca. Uni-verseg: Universal medical image segmentation. In *Proceedings of the IEEE/CVF International Conference on Computer Vision*, pages 21438–21451, 2023. [2](#)
- [10] Haoyu Cao, Tianyu Han, and Yunyun Yang. Hdnext: Hybrid dynamic mednext with level set regularization for medical image segmentation. In *Proceedings of the Asian Conference on Computer Vision*, pages 597–613, 2024. [2](#)
- [11] Dan Ciresan, Alessandro Giusti, Luca Gambardella, and Jürgen Schmidhuber. Deep neural networks segment neuronal membranes in electron microscopy images. *Advances in neural information processing systems*, 25, 2012. [4](#)
- [12] Jeffrey De Fauw, Joseph R Ledsam, Bernardino Romera-Paredes, Stanislav Nikolov, Nenad Tomasev, Sam Blackwell, Harry Askham, Xavier Glorot, Brendan O'Donoghue, Daniel Visentin, et al. Clinically applicable deep learning for

diagnosis and referral in retinal disease. *Nature medicine*, 24(9):1342–1350, 2018. 1

[13] Mostafa Dehghani, Josip Djolonga, Basil Mustafa, Piotr Padlewski, Jonathan Heek, Justin Gilmer, Andreas Peter Steiner, Mathilde Caron, Robert Geirhos, Ibrahim Alabdulmohsin, et al. Scaling vision transformers to 22 billion parameters. In *International conference on machine learning*, pages 7480–7512. PMLR, 2023. 2

[14] Jia Deng, Wei Dong, Richard Socher, Li-Jia Li, Kai Li, and Li Fei-Fei. Imagenet: A large-scale hierarchical image database. In *2009 IEEE conference on computer vision and pattern recognition*, pages 248–255. Ieee, 2009. 2

[15] Yang Deng, Ce Wang, Yuan Hui, Qian Li, Jun Li, Shiwei Luo, Mengke Sun, Quan Quan, Shuxin Yang, You Hao, Pengbo Liu, Honghu Xiao, Chunpeng Zhao, Xinpao Wu, and S. Kevin Zhou. Ctspine1k: A large-scale dataset for spinal vertebrae segmentation in computed tomography, 2024. 5

[16] Arjun D Desai, Andrew M Schmidt, Elka B Rubin, Christopher Michael Sandino, Marianne Susan Black, Valentina Mazzoli, Kathryn J Stevens, Robert Boutin, et al. Skm-tea: A dataset for accelerated mri reconstruction with dense image labels for quantitative clinical evaluation. In *Thirty-fifth Conference on Neural Information Processing Systems Datasets and Benchmarks Track (Round 2)*, 2021. 5

[17] Alexey Dosovitskiy, Lucas Beyer, Alexander Kolesnikov, Dirk Weissenborn, Xiaohua Zhai, Thomas Unterthiner, Mostafa Dehghani, Matthias Minderer, Georg Heigold, Sylvain Gelly, et al. An image is worth 16x16 words. *arXiv preprint arXiv:2010.11929*, 7:5, 2020. 15

[18] Yuxin Du, Fan Bai, Tiejun Huang, and Bo Zhao. Segvol: Universal and interactive volumetric medical image segmentation. *Advances in Neural Information Processing Systems*, 37:110746–110783, 2024. 5, 7

[19] Tugba Akinci D’Antonoli, Lucas K Berger, Ashraya K Indrakanti, Nathan Vishwanathan, Jakob Weiss, Matthias Jung, Zeynep Berkarda, Alexander Rau, Marco Reisert, Thomas Küstner, et al. Totalsegmentator mri: Robust sequence-independent segmentation of multiple anatomic structures in mri. *Radiology*, 314(2):e241613, 2025. 2, 3, 5, 7

[20] Yunhe Gao. Training like a medical resident: Context-prior learning toward universal medical image segmentation. In *Proceedings of the IEEE/CVF Conference on Computer Vision and Pattern Recognition*, pages 11194–11204, 2024. 3, 4

[21] Robert Graf, Paul-Sören Platzek, Evamaria Olga Riedel, Constanze Ramschütz, Sophie Starck, Hendrik Christian Möller, Matan Atad, Henry Völzke, Robin Bülow, Carsten Oliver Schmidt, et al. Totalvibesegmentator: Full body mri segmentation for the nako and uk biobank. *arXiv preprint arXiv:2406.00125*, 2024. 2, 3

[22] Endre Grøvik, Darvin Yi, Michael Iv, Elizabeth Tong, Daniel Rubin, and Greg Zaharchuk. Deep learning enables automatic detection and segmentation of brain metastases on multisequence mri. *Journal of Magnetic Resonance Imaging*, 51(1):175–182, 2020. 5

[23] Jie Gui, Tuo Chen, Jing Zhang, Qiong Cao, Zhenan Sun, Hao Luo, and Dacheng Tao. A survey on self-supervised learning: Algorithms, applications, and future trends. *IEEE Transactions on Pattern Analysis and Machine Intelligence*, 46(12):9052–9071, 2024. 2

[24] Ali Hatamizadeh, Vishwesh Nath, Yucheng Tang, Dong Yang, Holger R Roth, and Daguang Xu. Swin unetr: Swin transformers for semantic segmentation of brain tumors in mri images. In *International MICCAI brainlesion workshop*, pages 272–284. Springer, 2021. 4, 15

[25] Ali Hatamizadeh, Yucheng Tang, Vishwesh Nath, Dong Yang, Andriy Myronenko, Bennett Landman, Holger R Roth, and Daguang Xu. Unetr: Transformers for 3d medical image segmentation. In *Proceedings of the IEEE/CVF winter conference on applications of computer vision*, pages 574–584, 2022. 5, 15

[26] Yufan He, Pengfei Guo, Yucheng Tang, Andriy Myronenko, Vishwesh Nath, Ziyue Xu, Dong Yang, Can Zhao, Benjamin Simon, Mason Belue, et al. Vista3d: A unified segmentation foundation model for 3d medical imaging. In *Proceedings of the Computer Vision and Pattern Recognition Conference*, pages 20863–20873, 2025. 2, 3, 5, 7

[27] Nicholas Heller, Fabian Isensee, Dasha Trofimova, Resha Tejpaul, Zhongchen Zhao, Huai Chen, Lisheng Wang, Alex Golts, Daniel Khapun, Daniel Shats, et al. The kits21 challenge: Automatic segmentation of kidneys, renal tumors, and renal cysts in corticomedullary-phase ct. *arXiv preprint arXiv:2307.01984*, 2023. 3, 5

[28] Todd C Hollon, Balaji Pandian, Arjun R Adapa, Esteban Urias, Akshay V Save, Siri Sahib S Khalsa, Daniel G Eichberg, Randy S D’Amico, Zia U Farooq, Spencer Lewis, et al. Near real-time intraoperative brain tumor diagnosis using stimulated raman histology and deep neural networks. *Nature medicine*, 26(1):52–58, 2020. 1

[29] Le Hou, Dimitris Samaras, Tahsin M Kurc, Yi Gao, James E Davis, and Joel H Saltz. Patch-based convolutional neural network for whole slide tissue image classification. In *Proceedings of the IEEE conference on computer vision and pattern recognition*, pages 2424–2433, 2016. 4

[30] Ziyang Huang, Haoyu Wang, Zhongying Deng, Jin Ye, Yanzhou Su, Hui Sun, Junjun He, Yun Gu, Lixu Gu, Shaoting Zhang, et al. Stu-net: Scalable and transferable medical image segmentation models empowered by large-scale supervised pre-training. *arXiv preprint arXiv:2304.06716*, 2023. 2, 5, 7, 15

[31] Fabian Isensee, Paul F Jaeger, Simon AA Kohl, Jens Petersen, and Klaus H Maier-Hein. nnu-net: a self-configuring method for deep learning-based biomedical image segmentation. *Nature methods*, 18(2):203–211, 2021. 1, 5, 7, 9, 14, 15

[32] Fabian Isensee, Tassilo Wald, Constantin Ulrich, Michael Baumgartner, Saikat Roy, Klaus Maier-Hein, and Paul F Jaeger. nnu-net revisited: A call for rigorous validation in 3d medical image segmentation. In *International Conference on Medical Image Computing and Computer-Assisted Intervention*, pages 488–498. Springer, 2024. 1, 2, 3, 4, 5, 7, 14, 15

[33] Yuanfeng Ji, Haotian Bai, Chongjian Ge, Jie Yang, Ye Zhu, Ruimao Zhang, Zhen Li, Lingyan Zhanng, Wanling Ma, Xiang Wan, et al. Amos: A large-scale abdominal multi-organ

benchmark for versatile medical image segmentation. *Advances in neural information processing systems*, 35:36722–36732, 2022. 3, 5

[34] Longlong Jing and Yingli Tian. Self-supervised visual feature learning with deep neural networks: A survey. *IEEE transactions on pattern analysis and machine intelligence*, 43(11):4037–4058, 2020. 2

[35] Petr Jordan, Philip M Adamson, Vrunda Bhattbhatt, Surabhi Beriwal, Sangyu Shen, Oskar Radermecker, Supratik Bose, Linda S Strain, Michael Offe, David Fraley, et al. Pediatric chest-abdomen-pelvis and abdomen-pelvis ct images with expert organ contours. *Medical physics*, 49(5):3523–3528, 2022. 5

[36] Asifullah Khan, Zunaira Rauf, Abdul Rehman Khan, Saima Rathore, Saddam Hussain Khan, NajamusSaher Shah, Umair Farooq, Hifsa Asif, Aqsa Asif, Umme Zahoor, et al. A recent survey of vision transformers for medical image segmentation. *IEEE Access*, 2025. 1

[37] Bennett Landman, Zhoubing Xu, Juan Iglesias, Martin Styner, Thomas Langerak, and Arno Klein. Miccai multi-atlas labeling beyond the cranial vault–workshop and challenge. In *Proc. MICCAI multi-atlas labeling beyond cranial vault—workshop challenge*, page 12. Munich, Germany, 2015. 3, 5

[38] Ho Hin Lee, Shunxing Bao, Yuankai Huo, and Bennett A Landman. 3d ux-net: A large kernel volumetric convnet modernizing hierarchical transformer for medical image segmentation. *arXiv preprint arXiv:2209.15076*, 2022. 2, 4

[39] Wenxuan Li, Chongyu Qu, Xiaoxi Chen, Pedro RAS Bassi, Yijia Shi, Yuxiang Lai, Qian Yu, Huimin Xue, Yixiong Chen, Xiaorui Lin, et al. Abdomenatlas: A large-scale, detailed-annotated, & multi-center dataset for efficient transfer learning and open algorithmic benchmarking. *Medical Image Analysis*, 97:103285, 2024. 2

[40] Wenxuan Li, Alan Yuille, and Zongwei Zhou. How well do supervised 3d models transfer to medical imaging tasks? *arXiv preprint arXiv:2501.11253*, 2025. 2, 3

[41] Tsung-Yi Lin, Michael Maire, Serge Belongie, James Hays, Pietro Perona, Deva Ramanan, Piotr Dollár, and C Lawrence Zitnick. Microsoft coco: Common objects in context. In *European conference on computer vision*, pages 740–755. Springer, 2014. 2

[42] Geert Litjens, Thijs Kooi, Babak Ehteshami Bejnordi, Arnaud Arindra Adiyoso Setio, Francesco Ciompi, Mohsen Ghafoorian, Jeroen Awm Van Der Laak, Bram Van Ginneken, and Clara I Sánchez. A survey on deep learning in medical image analysis. *Medical image analysis*, 42:60–88, 2017. 1

[43] Bin Liu, Bing Li, Yaojing Chen, Victor Sreeram, and Shuofeng Li. Fast-mednext: Accelerating the mednext architecture to improve brain tumour segmentation efficiency. *International Journal of Imaging Systems and Technology*, 34(6):e23196, 2024. 2

[44] Jie Liu, Yixiao Zhang, Kang Wang, Mehmet Can Yavuz, Xiaoxi Chen, Yixuan Yuan, Haoliang Li, Yang Yang, Alan Yuille, Yucheng Tang, et al. Universal and extensible language-vision models for organ segmentation and tumor detection from abdominal computed tomography. *Medical image analysis*, 97:103226, 2024. 3

[45] Liyuan Liu, Haoming Jiang, Pengcheng He, Weizhu Chen, Xiaodong Liu, Jianfeng Gao, and Jiawei Han. On the variance of the adaptive learning rate and beyond. *arXiv preprint arXiv:1908.03265*, 2019. 5

[46] Zhuang Liu, Hanzi Mao, Chao-Yuan Wu, Christoph Feichtenhofer, Trevor Darrell, and Saining Xie. A convnet for the 2020s. In *Proceedings of the IEEE/CVF conference on computer vision and pattern recognition*, pages 11976–11986, 2022. 1

[47] Ilya Loshchilov, Frank Hutter, et al. Fixing weight decay regularization in adam. *arXiv preprint arXiv:1711.05101*, 5(5):5, 2017. 5

[48] Luca Lumetti, Vittorio Pipoli, Federico Bolelli, Elisa Ficarra, and Costantino Grana. Enhancing Patch-Based Learning for the Segmentation of the Mandibular Canal. *IEEE Access*, pages 1–12, 2024. 5

[49] Lena Maier-Hein, Matthias Eisenmann, Annika Reinke, Sinan Onogur, Marko Stankovic, Patrick Scholz, Tal Arbel, Hrvoje Bogunovic, Andrew P Bradley, Aaron Carass, et al. Why rankings of biomedical image analysis competitions should be interpreted with care. *Nature communications*, 9(1):5217, 2018. 1

[50] Shervin Minaee, Yuri Boykov, Fatih Porikli, Antonio Plaza, Nasser Kehtarnavaz, and Demetri Terzopoulos. Image segmentation using deep learning: A survey. *IEEE transactions on pattern analysis and machine intelligence*, 44(7):3523–3542, 2021. 1

[51] Andriy Myronenko. 3d mri brain tumor segmentation using autoencoder regularization. In *International MICCAI brain-tumor workshop*, pages 311–320. Springer, 2018. 15

[52] Ursula Nestle, Stephanie Kremp, Andrea Schaefer-Schuler, Christiane Sebastian-Welsch, Dirk Hellwig, Christian Rübe, and Carl-Martin Kirsch. Comparison of different methods for delineation of 18f-fdg pet-positive tissue for target volume definition in radiotherapy of patients with non-small cell lung cancer. *Journal of nuclear medicine*, 46(8):1342–1348, 2005. 1

[53] Florian Putz, Sogand Beirami, Manuel Alexander Schmidt, Matthias Stefan May, Johanna Grigo, Thomas Weissmann, Philipp Schubert, Daniel Höfler, Ahmed Gomaa, Ben Tkhayat Hassen, et al. The segment anything foundation model achieves favorable brain tumor auto-segmentation accuracy in mri to support radiotherapy treatment planning. *Strahlentherapie und Onkologie*, 201(3):255–265, 2025. 3

[54] Chongyu Qu, Tiezheng Zhang, Hualin Qiao, Yucheng Tang, Alan L Yuille, Zongwei Zhou, et al. Abdomenatlas-8k: Annotating 8,000 ct volumes for multi-organ segmentation in three weeks. *Advances in Neural Information Processing Systems*, 36:36620–36636, 2023. 2, 5, 14

[55] Alec Radford, Jong Wook Kim, Chris Hallacy, Aditya Ramesh, Gabriel Goh, Sandhini Agarwal, Girish Sastry, Amanda Askell, Pamela Mishkin, Jack Clark, et al. Learning transferable visual models from natural language supervision. In *International conference on machine learning*, pages 8748–8763. PMLR, 2021. 2

[56] Md Mostafijur Rahman, Mustafa Munir, and Radu Mărușescu. Efficientmednext: Multi-receptive dilated convolutions for medical image segmentation. In *International Conference on Medical Image Computing and Computer-Assisted Intervention*, pages 196–206. Springer, 2025. 2

[57] Tal Ridnik, Emanuel Ben-Baruch, Asaf Noy, and Lih Zelnik-Manor. Imagenet-21k pretraining for the masses. *arXiv preprint arXiv:2104.10972*, 2021. 5

[58] Maximilian Rokuss, Yannick Kirchhoff, Seval Akbal, Balint Kovacs, Saikat Roy, Constantin Ulrich, Tassilo Wald, Lukas T Rotkopf, Heinz-Peter Schlemmer, and Klaus Maier-Hein. Lesionlocator: Zero-shot universal tumor segmentation and tracking in 3d whole-body imaging. In *Proceedings of the Computer Vision and Pattern Recognition Conference*, pages 30872–30885, 2025. 2

[59] Olaf Ronneberger, Philipp Fischer, and Thomas Brox. U-net: Convolutional networks for biomedical image segmentation. In *International Conference on Medical image computing and computer-assisted intervention*, pages 234–241. Springer, 2015. 1, 4

[60] Saikat Roy, David Kügler, and Martin Reuter. Are 2.5 d approaches superior to 3d deep networks in whole brain segmentation? In *International Conference on Medical Imaging with Deep Learning*, pages 988–1004. PMLR, 2022. 4

[61] Saikat Roy, Gregor Koehler, Constantin Ulrich, Michael Baumgartner, Jens Petersen, Fabian Isensee, Paul F Jaeger, and Klaus H Maier-Hein. Mednext: transformer-driven scaling of convnets for medical image segmentation. In *International Conference on Medical Image Computing and Computer-Assisted Intervention*, pages 405–415. Springer, 2023. 2, 3, 4, 5, 7, 14, 15

[62] Saikat Roy, Tassilo Wald, Michael Baumgartner, Constantin Ulrich, Gregor Koehler, David Zimmerer, Fabian Isensee, and Klaus Maier-Hein. Lost in transformation: Current roadblocks for transformers in 3d medical image segmentation. 2023. 2

[63] Saikat Roy, Mahmoud Mostapha, Radu Miron, Matt Holbrook, and Mariappan Nadar. Investigating the feasibility of patch-based inference for generalized diffusion priors in inverse problems for medical images. In *2025 IEEE 22nd International Symposium on Biomedical Imaging (ISBI)*, pages 1–4. IEEE, 2025. 4

[64] Julio Silva-Rodríguez, Jose Dolz, and Ismail Ben Ayed. Towards foundation models and few-shot parameter-efficient fine-tuning for volumetric organ segmentation. In *International Conference on Medical Image Computing and Computer-Assisted Intervention*, pages 213–224. Springer, 2023. 3

[65] Simon John Christoph Soerensen, Richard E Fan, Arun Seetharaman, Leo Chen, Wei Shao, Indrani Bhattacharya, Yong-hun Kim, Rewa Sood, Michael Borre, Benjamin I Chung, et al. Deep learning improves speed and accuracy of prostate gland segmentations on magnetic resonance imaging for targeted biopsy. *The Journal of urology*, 206(3):604–612, 2021. 3

[66] Chen Sun, Abhinav Shrivastava, Saurabh Singh, and Abhinav Gupta. Revisiting unreasonable effectiveness of data in deep learning era. In *Proceedings of the IEEE international conference on computer vision*, pages 843–852, 2017. 2, 5

[67] Mingxing Tan and Quoc Le. Efficientnet: Rethinking model scaling for convolutional neural networks. In *International conference on machine learning*, pages 6105–6114. PMLR, 2019. 4

[68] Constantin Ulrich, Fabian Isensee, Tassilo Wald, Maximilian Zenk, Michael Baumgartner, and Klaus H Maier-Hein. Multitalent: A multi-dataset approach to medical image segmentation. In *International Conference on Medical Image Computing and Computer-Assisted Intervention*, pages 648–658. Springer, 2023. 2

[69] Tassilo Wald, Saikat Roy, Fabian Isensee, Constantin Ulrich, Sebastian Ziegler, Dasha Trofimova, Raphael Stock, Michael Baumgartner, Gregor Köhler, and Klaus Maier-Hein. Primus: Enforcing attention usage for 3d medical image segmentation. *arXiv preprint arXiv:2503.01835*, 2025. 8

[70] Tassilo Wald, Constantin Ulrich, Stanislav Lukyanenko, Andrei Goncharov, Alberto Paderno, Maximilian Miller, Leander Maerkisch, Paul Jaeger, and Klaus Maier-Hein. Revisiting mae pre-training for 3d medical image segmentation. In *Proceedings of the Computer Vision and Pattern Recognition Conference*, pages 5186–5196, 2025. 2

[71] Tassilo Wald, Constantin Ulrich, Jonathan Suprijadi, Sebastian Ziegler, Michal Nohel, Robin Peretzke, Gregor Kohler, and Klaus Maier-Hein. An openmind for 3d medical vision self-supervised learning. In *Proceedings of the IEEE/CVF International Conference on Computer Vision*, pages 23839–23879, 2025. 2

[72] Haoyu Wang, Sizheng Guo, Jin Ye, Zhongying Deng, Junlong Cheng, Tianbin Li, Jianpin Chen, Yanzhou Su, Ziyan Huang, Yiqing Shen, et al. Sam-med3d: towards general-purpose segmentation models for volumetric medical images. In *European Conference on Computer Vision*, pages 51–67. Springer, 2024. 2, 3

[73] Jakob Wasserthal, Hanns-Christian Breit, Manfred T Meyer, Maurice Pradella, Daniel Hinck, Alexander W Sauter, Tobias Heye, Daniel T Boll, Joshy Cyriac, Shan Yang, et al. Totsalsegmentator: robust segmentation of 104 anatomic structures in ct images. *Radiology: Artificial Intelligence*, 5(5):e230024, 2023. 2, 3, 5, 7

[74] Sanghyun Woo, Shoubhik Debnath, Ronghang Hu, Xinlei Chen, Zhuang Liu, In So Kweon, and Saining Xie. Convnext v2: Co-designing and scaling convnets with masked autoencoders. In *Proceedings of the IEEE/CVF conference on computer vision and pattern recognition*, pages 16133–16142, 2023. 3, 4, 6

[75] Yutong Xie, Jianpeng Zhang, Chunhua Shen, and Yong Xia. Cotr: Efficiently bridging cnn and transformer for 3d medical image segmentation. In *International conference on medical image computing and computer-assisted intervention*, pages 171–180. Springer, 2021. 15

[76] Murong Xu, Tamaz Amiranashvili, Fernando Navarro, Maksym Fritsak, Ibrahim Ethem Hamamci, Suprosanna Shit, Bastian Wittmann, Sezgin Er, Sebastian M Christ, Ezequiel de la Rosa, et al. Cads: A comprehensive anatomical

dataset and segmentation for whole-body anatomy in computed tomography. *arXiv preprint arXiv:2507.22953*, 2025. [2](#), [3](#), [5](#), [7](#), [14](#)

[77] Bolei Zhou, Hang Zhao, Xavier Puig, Sanja Fidler, Adela Barriuso, and Antonio Torralba. Scene parsing through ade20k dataset. In *Proceedings of the IEEE conference on computer vision and pattern recognition*, pages 633–641, 2017. [2](#)

# MedNeXt-v2: Scaling 3D ConvNeXts for Large-Scale Supervised Representation Learning in Medical Image Segmentation

## Supplementary Material

### A. Large-scale pretrained models in literature

There have been a plethora of deep learning architectures with large-scale supervised pretraining in 3D medical image segmentation. We use seven such architectures in our benchmarking in Tab. 4. The models are described briefly with their backbone architecture as follows:

1. **TotalSegmentator:** TotalSegmentator is an nnUNet [31] architecture trained on 1228 CT images with 117 anatomical structures.
2. **MRSegmentator:** MRSegmentator is an nnUNet architecture trained on 616 volumes with 50 anatomical structures. The project is jointly maintained as part of TotalSegmentator.
3. **CADS:** CADS presents a ResEncL nnUNet [32] trained on a collection of 22022 CT volumes. While each volume contains 167 annotated structures, the pretrained weights are made available for major anatomical subsets of structures. We use the pretrained weights for subset 1 defined as “*major abdominal organs, primary thoracic organs (lungs), and major abdominal vasculature*” [76] in the course of this work.
4. **Vista3D:** Vista3D uses a modified SegResNet backbone trained on 11454 CT volumes with 127 classes, designed to perform both automatic and interactive segmentation. For the purposes of this work, we retrained the segmentation branch while deactivating the interactive branch.
5. **SegVol:** SegVol uses a 3D ViT image encoder which is pretrained on 96000 CT volumes followed by finetuning on 6000 CTs on 47 anatomical areas. The ViT is utilized as part of an UNETR image encoder following instruction on the SegVol Github repository.
6. **STUNet-L:** STU-Net uses a modified and significantly scaled up nnUNet variant as the backbone of its work. The pretrained weights are derived from the weights made publicly available by the authors following their participation in the Touchstone benchmark [4].
7. **MedNeXt-v1:** MedNeXt-v1 used in the pretrained model section of Tab. 4 has been pretrained on AbdomenAtlas1.0 [54] which consists of 5195 Abdomen CT volumes with 10 annotated abdominal structures.

### B. MedNeXt-v2 architecture

The macro architecture of MedNeXt-v2 is similar to that of MedNeXt-v1 [61]. The architecture is symmetrical in terms of encoder and decoder capacities, consists of 5 spatial hierarchies, each with  $B_i$  blocks and leverages deep supervision

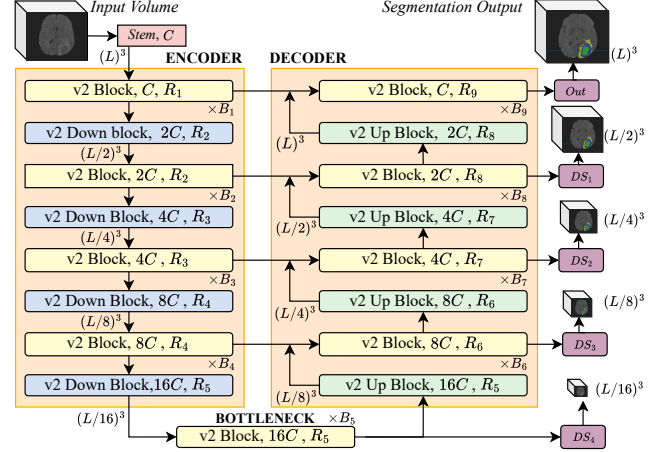


Figure 8. **MedNeXt-v2 architecture.** The macro-architecure of MedNeXt-v2 is fundamentally similar to that of MedNeXt-v1 [61]. The differences lie in the unique benefits of mirco-architectural changes via the GRN, architecture scaling and leveraging large-scale supervised pretraining for state-of-the-art 3D medical image segmentation.

at all levels of the decoder. All residuals are additive and all layers benefit from GRN as described in Sec. 2.2.1, including the up and downsampling layers. The layers in Fig. 8 are described as follows:

1. **Stem:** The *Stem* is designed to use a Conv3d of kernel size and stride of 1 to project the input channels into the base number of channels ( $C$ ) of the architecture.
2. **MedNeXt-v2 block:** The *MedNeXt-v2 block* is a residual ConvNeXt block which has the following operations in sequence – a depthwise convolution layer with convolution kernel size 3, an instance norm layer, a pointwise expansion convolution with an expansion ratio  $R$ , a GELU activation, a GRN block and a pointwise compression convolution reducing the channels to the base number of channels for the layer. The nomenclature (v2 Block,  $4C$ ,  $R_7$ ) in Fig. 8 indicates that the convolution operation of the block has an input and output of channel count of  $4C$  with an expansion ratio of  $R_7$  per the architecture configurations (derived from MedNeXt-v1).
3. **MedNeXt-v2 Up/Down Block:** The *MedNeXt-v2 Up/Down blocks* (see Fig. 2) differ from the standard *MedNeXt-v2 blocks* merely in strided convolutions in the depthwise block with Transposed Convolutions replacing the normal Convolution operation in the upsampling layers. There is also a doubling of channels following

downsampling and halving following upsampling as in most UNet architectures. There is also a convolution or strided convolution in the residual connection to adjust the spatial and channel dimensions.

4. **Deep Supervision (DS) / Output (Out) Block:** Each DS or Out block is merely a convolution of kernel size 1 mapping the number of channels of the input tensor to the number of output classes of the task.

## C. Backbone Benchmarking models

We use nnUNet [31], SegResNet [51], ResEncL [32], SwinUNETR [24] and UNETR [25] which is the representative popular backbone architecture using a Vision Transformer (ViT) [17]. Competing state-of-the-art methods include MedNeXt (v1) [61], STU-Net [30] and CoTr [75], where each method is a high performer in recent small and large-scale benchmarks for 3D medical image segmentation [4, 32].

## D. Datasets

We use a pool of *validation datasets* to validate our backbone prior to architecture scaling (Sec. 2.1) on which we report results on a single 80:20 split. We keep these separate from our set of 6 final datasets where we perform more extensive 5-fold cross validation in Tab. 4, to avoid optimizing our backbone on our test data.

### D.1. Validation Datasets

Our validation dataset pool consists of four popular public dataset (3 CT and 1 cineMRI) as used in [32, 61]. They are described briefly in the following:

1. *BTCV*: The *Beyond-The-Cranial-Vault (BTCV)* is a small but popular dataset consisting of 30 CT images with 13 annotated abdominal organs.
2. *AMOS22*: The *AMOS22* competition dataset consists of 200 abdominal CT volumes with 15 annotated organs. This is the version of the dataset used prior to the completion of the AMOS22 Grand Challenge and has been used to retain parity with MedNeXt-v1.
3. *KiTS23*: The *Kidney Tumor Segmentation (KiTS23)* challenge 2023 dataset consists of 489 volumes of 2 annotated labels of kidney and tumor.
4. *ACDC*: The *ACDC* dataset consists of 200 samples of cineMRI volumes with 3 annotated labels for heart structures.

## E. The diminishing returns of scaling in 3D medical image segmentation

Following up on our network scaling experiments with MedNeXt-v2 (Sec. 4.1), we observe that certain datasets, such as Stanford Knee MR (D2), exhibit substantial saturation. The standard deviation across all methods is 0.43

DSC and 0.8 NSD, excluding the lowest-performing SegVol model, these values drop to 0.10 DSC and 0.17 NSD. In fact, there is barely any difference between nnU-Net trained from scratch and any pretrained model, regardless of scale and especially in terms of DSC which focuses on volumetric accuracy. Importantly, this phenomenon occurs in only one of the six datasets in our final evaluation pool. This strongly suggests that the benefits of model scaling and pretraining, while generally positive, cannot reliably overcome inherent performance saturation present in some datasets. As a result, careful consideration is needed when selecting evaluation data as well as depending on just a single metric for large-scale pretrained models, since saturated datasets may lead to inconclusive assessments of pretraining efficacy in future benchmarks.

This is also demonstrated in mixed performance of some datasets with the 30M parameter TotalSegmentator model sometimes having similar finetuning performance as the 440M parameter STU-Net model – importantly, both share the same ConvNet-based nnUNet backbone. However, the 247M parameter MedNeXt-v2 (Width  $\times$  2.0) model is often noticeably better than both TotalSegmentator and STU-Net, which indicates that the architecture design (ConvNet vs ConvNeXt) might also be a factor in architecture scaling. Merely scaling the network parameters, while sometimes effective, might lead to saturation of performance but can be overcome with better backbone architecture design.